Scan Registration for Mechanical Scanning Imaging Sonar Using kD2D-NDT

Min Jiang[1,2], Sanming Song[1], Yiping Li[1], Jian Liu[1], Xisheng Feng[1]

1. State Key Laboratory of Robotics, Shenyang Institute of Automation, Chinese Academy of Sciences, Shenyang 110016, China

2. University of Chinese Academy of Sciences, Beijing 100049, China

E-mail: {jiangmin,songsanming,lyp,liuj,fxs}@sia.cn

Abstract: A method derived from the D2D-NDT, named kD2D-NDT, is proposed to register the scans that are collected by the Mechanical Scanning Imaging Sonar (MSIS). The D2D-NDT method replaces the point-to-distribution (P2D) scoring in the normal distribution transformation (NDT) with distribution-to-distribution (D2D) matching, greatly reducing the computation cost. In this paper, several heuristic strategies are adopted in kD2D-NDT to accelerate and stabilize the matching process. Firstly, the point cloud of the *floating* scan and the *reference* scan are grouped into compact clusters by the *K-means* clustering method to accommodate the Gaussian mixture model assumption which underlies the D2D distance measure and no iterative optimization at different grid size is needed. Secondly, for each Gaussian component in the *floating* scan, only $k = 3$ nearest Gaussian components in the *reference* scan are chosen to measure the similarity. Lastly, to avoid the singularity in calculating the matrix inverse, the Euclidean distance between the centroid pair, instead of the Mahalanobis distance, is adopted to find the most similar Gaussian components. Its applications to the scans that are collected from the realistic underwater environment show that the proposed strategies make kD2D-NDT practical for the MSIS scans.

Key Words: scan registration, kD2D-NDT, mechanical scanning imaging sonar

1 Introduction

In ocean engineering, optical sensors have been widely used in observing the underwater structure and seabed. For example, in the oceanographic applications like coral reefs observation [1], shipwrecks or archaeological significance sites imaging [2], high-resolution optical images have been collected to support the relevant scientific investigations. However, there are large quantities of planktons and evoked mud, sands in the realistic ocean water column, which severely shorten the visual distance of the optical sensors. Instead, the acoustic sensors, for example, the forward-looking sonars, which perceive the surrounding environments by transmitting the ultrasonic wave and receiving the reverberations, are able to penetrate the turbid water. Therefore, they have been widely used in underwater environment.

Mechanical Scanning Imaging Sonar(MSIS), a kind of acoustic sensors, is extensively equipped by small autonomous underwater vehicles (AUVs) and remotely-operated vehicle (ROVs) because of its low cost, low power consumption and compact size. Each time, MSIS emits a beam in a certain direction and the receiver waits an echoic response for a certain time due to the eventual rebound of sound to intercept an object in its path. Then, MSIS changes the sender direction in an angular step, emits a beam again and waits for the corresponding response. This process is repeated to cover the entire scan sector [3]. Zhou et al. [4] equipped an underwater Slocum glider with the MSIS to profile underwater iceberg. Franco et al. [3] used MSIS to avoid the obstacles in the AUV platform. Mallios et al. [5] installed two MSIS on an AUV, one horizontal and one vertical, operating simultaneously to generate 3D map of the underwater caves.

A basic problem in acoustic vision is to construct a panoramic map by stitching the scans that are collected by the sonar at different times [6–9]. In fact, the scan registration, which is also known as data association and helps to correct the accumulated error in the dead-reckoning process, has been considered as an indispensable component of the well-known SLAM (simultaneous localization and mapping) system. SLAM is considered as one of the fundamental problems that need to be solved before achieving truly autonomous robots. SLAM techniques have been broadly and successfully applied to terrestrial robots and aerial robots. However, due to the great difficulties in data association, little progress has been achieved in the underwater environment.

Registration methods that rely on the feature extraction, like point feature [10] and line feature [11], have been proved to be unavailable when MSIS working in unstructured environment, because it is very difficult to extrac-

The work is supported by the National Natural Science Foundation of China (No. 41506121), the National Key Research and Development Program of China (No. 2017YFC0305901, No. 2016YFC0300604, No. 2016YFC0301601), the Strategic Priority Program of the Chinese Academy of Sciences (No. XDA13030205, No. XDA11040103), the State Key Laboratory of Robotics of China (No. 2017-Z010), the project of "R&D Center for Underwater Construction Robotics", funded by the Ministry of Ocean and Fisheries (MOF) and Korea Institute of Marine Science & Technology Promotion (KIMST), Korea (No. PJT200539), the Public science and technology research funds projects of ocean (No. 201505017).

978-1-5386-1243-9/18/$31.00

t structured features from the sonar images that are taken from the unstructured natural underwater environment. Therefore, featureless methods, for example, scan matching have successfully attracted the attention of underwater community. Castellani et al. [12] proposed an ICP-based method to register 3D acoustic camera images. Hernndez et al. [13] proposed another variant of ICP method, the M-SISpIC, to solve the registration problem with distortion in the acoustic image brought by vehicle motion during a scan circle. On another hand, Buelow et al [14] presented a spectral registration method to achieve fast and robust scan matching. Its application to 3D sonar images is reported in [15]. It is worthy to mention that Chen et al [16] have ever adopted the scan matching to calculate constraints in constructing pose graph.

Traditional methods usually only preserve the highest-intensity bins that correspond to objects in the scene, abandoning the rest of opaque returns. With respect to the uncertainties underlying the acoustic measurements, it is more appropriate to make full use of the available information. On another hand, the computation cost will rapidly grow if a point-to-point (P2P for short) matching method is adopted to perform the scan registration. Furthermore, the matching points may not correspond to the same point in the physical world. Therefore, it is helpful to solve the registration problem in probabilistic framework. For example, in the NDT method [17], the 2D sonar scan is divided into equal-sized blocks and each block is described by a Gaussian distribution. In the registration step, a probability score is obtained when each point in the *floating* scan is mapped to the nearest Gaussian distribution in the *reference* scan (point-to-distribution matching, P2D for short). An optimal or suboptimal transformation parameter set could be pursued by maximizing the accumulated probability score with a selected optimization strategy. To further reduce the computation cost in the P2D-based NDT method, a distribution-to-distribution (D2D for short) method which directly measures the distance between two Gaussian distributions has been proposed by [18] to register the lidar point clouds.

However, the D2D-NDT method suffers the following two problems in registering the sonar scans. On one hand, the point distribution in a block may be not appropriate to be described by a Gaussian distribution. It demonstrates that a deliberate block division strategy should be designed to better accommodate the Gaussian distribution. On the other hand, measure the distance between all the components in the *floating* scan to all the Gaussian components in the *reference* scan will smooth the differences between two sonar scans. To make it practical for the underwater sonar scan registration, several strategies are proposed to accelerate and stabilize the matching process. Firstly, the cloud points in each scan are grouped into compact clusters by the *K-means* clustering method to accommodate the Gaussian mixture model assumption. Secondly, only $k = 3$ nearest Gaussian components, instead of all the Gaussian components, in the *reference* scan are used to measure the similarity. Lastly, the Euclidean distance is adopted to find the most similar k Gaussian components. For simplicity, the method is called kD2D-NDT in the following sections.

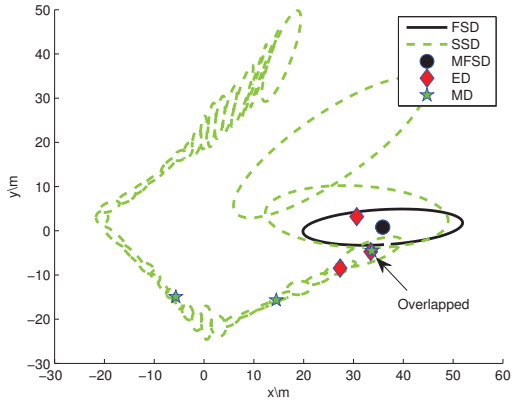

Figure 1: An example for Gaussian candidates in *reference* scan selected by different similarity measure. The Gaussian component in the *floating* scan is represented by a black ellipse. The most similar $k = 3$ Gaussian components found by the Euclidean distance and Mahalanobis distance are shown by red diamond and green five-start respectively.

The paper is organized as follows: The kD2D-NDT method is introduced in Section 2, and its application to the realistic underwater sonar scans is reported in Section 3. Section 4 concludes the paper and provides some interesting discussions on our future work on the NDT methods.

2 kD2D-NDT Registration

Consider a *floating* scan F and a *reference* scan R that are taken by the MSIS forward-looking sonar at different times. If the scans are overlapping, there should be a transformation function T, which is parameterized by the parameter set $\boldsymbol{p} = (t_x, t_y, \theta)^T$, mapping each point in F to its counterpart in R consistently.

If we group the point clouds into several compact clusters with the *K-means* clustering method, each scan can be described by a Gaussian mixture model, i.e. $\mathcal{G}_F$ and $\mathcal{G}_R$, where each component corresponds to a cluster.

Then, an analytical object function, which measures the similarity between two Gaussian mixture models, could be designed to pursue the transformation parameters, using $\mathcal{L}_2$ norm.

The $\mathcal{L}_2$ distance between two Gaussian mixture models $\mathcal{G}_F$ and $\mathcal{G}_R$ with transformation parameter set $\boldsymbol{p}$ is defined as

$$\mathcal{D}_{L_2}(F, R, \boldsymbol{p}) = \int \left(p(\boldsymbol{x}|\mathcal{G}_F) - p(\boldsymbol{x}|T(\mathcal{G}_R, \boldsymbol{p}))\right)^2 \mathrm{d}\boldsymbol{x} \quad . \tag{1}$$

With simple mathematical manipulations, it can be simplified as

$$\mathcal{D}_{L_2}(F, R, \boldsymbol{p}) \sim \sum_{i=1}^{n_F} \sum_{j=1}^{n_R} N(0|T(\boldsymbol{\mu}_i, \boldsymbol{p}) - \boldsymbol{\mu}_j, T(\Sigma_i, \boldsymbol{p}) + \Sigma_j) \tag{2}$$

where n_F and n_R are the number of Gaussian components in $\mathcal{G}_F$ and $\mathcal{G}_R$ respectively.

Empirically, there is no need to consider the similarity measure between each Gaussian component in the *floating* scan and all the components in the *reference* scan. In fact, a catastrophic effect is that such a scheme easily smooths the differences between two sonar scans. In our implementation, for each Gaussian component $N(\boldsymbol{\mu}_i, \Sigma_i)$ in the *floating* scan F, only three nearest Gaussian components in the *reference* scan R were experimentally chosen to measure the similarity between two scans. It should be noted that the Euclidean distance between the centroid pair, instead of the Mahalanobis distance in the NDT method [17], was adopted to find the most similar Gaussian components. Experiments show that the Euclidean distance benefits the stabilities of the D2D-NDT algorithm. In this case, the objective function (2) is rewritten as

$$\mathcal{F}_{d2d}(\boldsymbol{p}) = \sum_{i=1}^{n_F}\sum_{j=1}^{n_{R_3}} -d_1 \exp(-\frac{d_2}{2}\boldsymbol{\mu}_{ij}^T B \boldsymbol{\mu}_{ij}) \tag{3}$$

where $\boldsymbol{\mu}_{ij} = \boldsymbol{\mu}_{ij}(\boldsymbol{p}) = R\boldsymbol{\mu}_i + \boldsymbol{t} - \boldsymbol{\mu}_j$, and $\boldsymbol{\mu}_i = [\mu_{ix}, \mu_{iy}]^T, \boldsymbol{\mu}_j = [\mu_{jx}, \mu_{jy}]^T$.
The optimal transformation parameters can be solved by minimizing the objective function (3) with a special gradient descent strategy, for example, the Newton's method,

$$\Delta \boldsymbol{p} = -\eta \frac{\nabla \mathcal{F}(\mathbf{p})}{\nabla \mathcal{F}^2(\mathbf{p})}, \tag{4}$$

where $\nabla \mathcal{F}(\mathbf{p})$ and $\nabla \mathcal{F}^2(\mathbf{p})$ are the gradient and Hessian matrix respectively, η is the learning rate.
The gradient of objective function is

$$\nabla \mathcal{F}(\boldsymbol{p}) = \frac{C}{2}\begin{pmatrix} 2\boldsymbol{\mu}_{ij}^T B \boldsymbol{j}_1 \\ 2\boldsymbol{\mu}_{ij}^T B \boldsymbol{j}_2 \\ 2\boldsymbol{\mu}_{ij}^T B \boldsymbol{j}_3 - \boldsymbol{\mu}_{ij}^T B Z_3 B \boldsymbol{\mu}_{ij} \end{pmatrix} \tag{5}$$

where

$$B = (R^T \Sigma_i R + \Sigma_j)^{-1} \tag{6}$$

$$C = d_1 d_2 \exp\left(-\frac{d_2 \boldsymbol{\mu}_{ij}^T B \boldsymbol{\mu}_{ij}}{2}\right) \tag{7}$$

$$\boldsymbol{j}_1 = \frac{\partial}{\partial p_1}\boldsymbol{\mu}_{ij}(\boldsymbol{p}) = \begin{pmatrix} 1 \\ 0 \end{pmatrix} \tag{8}$$

$$\boldsymbol{j}_2 = \frac{\partial}{\partial p_2}\boldsymbol{\mu}_{ij}(\boldsymbol{p}) = \begin{pmatrix} 0 \\ 1 \end{pmatrix} \tag{9}$$

$$\boldsymbol{j}_3 = \frac{\partial}{\partial p_3}\boldsymbol{\mu}_{ij}(\boldsymbol{p}) = \begin{pmatrix} -\mu_{ix}\sin\theta - \mu_{iy}\cos\theta \\ \mu_{ix}\cos\theta - \mu_{iy}\sin\theta \end{pmatrix} \tag{10}$$

and p_a is a component of the transformation parameter vector $\boldsymbol{p}$.
The components of the Hessian matrix

$$\nabla \mathcal{F}^2(\boldsymbol{p}) = \begin{bmatrix} H_{11} & H_{12} & H_{13} \\ H_{21} & H_{22} & H_{23} \\ H_{31} & H_{32} & H_{33} \end{bmatrix} \tag{11}$$

are given by the following 9 equations.

$$H_{11} = C\left(\boldsymbol{j}_1^T B \boldsymbol{j}_1 - d_2\left(\boldsymbol{\mu}_{ij}^T B \boldsymbol{j}_1\right)^2\right) \tag{12}$$

$$H_{12} = C\left(\boldsymbol{j}_2^T B \boldsymbol{j}_1 - d_2\left(\boldsymbol{\mu}_{ij}^T B \boldsymbol{j}_2\right)\left(\boldsymbol{\mu}_{ij}^T B \boldsymbol{j}_1\right)\right) \tag{13}$$

$$H_{13} = C\left(\boldsymbol{j}_3^T B \boldsymbol{j}_1 - \boldsymbol{\mu}_{ij}^T B Z_3 B \boldsymbol{j}_1 - \frac{d_2}{2}\left(2\boldsymbol{\mu}_{ij}^T B \boldsymbol{j}_3 - \boldsymbol{\mu}_{ij}^T B Z_3 B \boldsymbol{\mu}_{ij}\right)\left(\boldsymbol{\mu}_{ij}^T B \boldsymbol{j}_1\right)\right) \tag{14}$$

$$H_{21} = C\left(\boldsymbol{j}_1^T B \boldsymbol{j}_2 - d_2\left(\boldsymbol{\mu}_{ij}^T B \boldsymbol{j}_1\right)\left(\boldsymbol{\mu}_{ij}^T B \boldsymbol{j}_2\right)\right) \tag{15}$$

$$H_{22} = C\left(\boldsymbol{j}_2^T B \boldsymbol{j}_2 - d_2\left(\boldsymbol{\mu}_{ij}^T B \boldsymbol{j}_2\right)^2\right) \tag{16}$$

$$H_{23} = C\left(\boldsymbol{j}_3^T B \boldsymbol{j}_2 - \boldsymbol{\mu}_{ij}^T B Z_3 B \boldsymbol{j}_2 - \tfrac{d_2}{2}\left(2\boldsymbol{\mu}_{ij}^T B \boldsymbol{j}_3 - \boldsymbol{\mu}_{ij}^T B Z_3 B \boldsymbol{\mu}_{ij}\right)\left(\boldsymbol{\mu}_{ij}^T B \boldsymbol{j}_2\right)\right) \tag{17}$$

$$H_{31} = \tfrac{C}{2}\left(2\boldsymbol{j}_1^T B \boldsymbol{j}_3 - 2\boldsymbol{\mu}_{ij}^T B Z_3 B \boldsymbol{j}_1 - d_2\left(2\boldsymbol{\mu}_{ij}^T B \boldsymbol{j}_3 - \boldsymbol{\mu}_{ij}^T B Z_3 B \boldsymbol{\mu}_{ij}\right)\left(\boldsymbol{\mu}_{ij}^T B \boldsymbol{j}_1\right)\right) \tag{18}$$

$$H_{32} = \tfrac{C}{2}\left(2\boldsymbol{j}_2^T B \boldsymbol{j}_3 - 2\boldsymbol{\mu}_{ij}^T B Z_3 B \boldsymbol{j}_2 - d_2\left(2\boldsymbol{\mu}_{ij}^T B \boldsymbol{j}_3 - \boldsymbol{\mu}_{ij}^T B Z_3 B \boldsymbol{\mu}_{ij}\right)\left(\boldsymbol{\mu}_{ij}^T B \boldsymbol{j}_2\right)\right) \tag{19}$$

$$H_{33} = \tfrac{C}{2}\left(2\boldsymbol{j}_3^T B \boldsymbol{j}_3 - 4\boldsymbol{\mu}_{ij}^T B Z_3 B \boldsymbol{j}_3 + 2\boldsymbol{\mu}_{ij}^T B \boldsymbol{j}_{33} + 2\boldsymbol{\mu}_{ij}^T B Z_3 B Z_3 B \boldsymbol{\mu}_{ij} - \boldsymbol{\mu}_{ij}^T B Z_{33} B \boldsymbol{\mu}_{ij} - \tfrac{d_2}{2}\left(2\boldsymbol{\mu}_{ij}^T B \boldsymbol{j}_3 - \boldsymbol{\mu}_{ij}^T B Z_3 B \boldsymbol{\mu}_{ij}\right)^2\right) \tag{20}$$

Note that the 5 auxiliary variables are expressed in the following equations.

$$Z_1 = \frac{\partial}{\partial p_1}(R^T \Sigma_i R) \tag{21}$$

$$Z_2 = \frac{\partial}{\partial p_2}(R^T \Sigma_i R) \tag{22}$$

$$Z_3 = \frac{\partial}{\partial p_3}(R^T \Sigma_i R) \tag{23}$$

$$Z_{33} = \frac{\partial^2}{\partial p_3^2}(R^T \Sigma_i R) \tag{24}$$

$$\boldsymbol{j}_{33} = \frac{\partial^2}{\partial p_3^2}\boldsymbol{\mu}_{ij}(\boldsymbol{p}) \tag{25}$$

3 EXPERIMENTS

In this section, we used the dataset collected in an abandoned marina located in the Catalan coast [19] to test the feasibility of kD2D-NDT for the underwater sonar scans of the MSIS sonar. For each beam of a scan, only those bins with an intensity higher than a threshold were preserved, i.e.$TH = 80$. As in [20], the location and pose of the AUV, which were collected by the inertial navigation system, were used to correct the distortion brought by the movement or perturbation of the vehicle.
In the following three tests, the parameters $d1$,$d2$ were empirically set to 1 and 0.01 for D2D-NDT, the learning rate of Newtonian method was set to 0.5 for D2D-NDT and 1 for P2D-NDT. Initial transformation parameter was $(0, 0, 0)$. Each cluster that was generated by the *K-means* clustering algorithm was described by a Gaussian model. For easier visualization, the Gaussian model was presented

Table 1: Estimate motion parameters for a known sonar image pair with different registration methods

Estimation	True parameters	kD2D	D2D	ICP	P2D
x	-1.569603	-1.667668	-1.735926	-1.037067	-1.568309
y	-2.5359	-2.516987	-2.504602	-2.553541	-2.491915
$\theta(degree)$	4.06563	3.972754	4.875901	3.036055	3.786512

Table 2: Average estimation error and runtime comparison for different registration methods

Error and Runtime	Δx	Δy	$\Delta\theta(degree)$	$Runtime(second)$
kD2D	-0.1773±0.8296	0.0383±0.3466	-0.1076±1.4620	0.4895±0.2924
D2D	-0.3840±2.0720	-0.0184±0.9736	0.0583±1.5779	6.4322±2.6781
ICP	-0.0306±0.6869	0.0403±0.2349	0.0628±1.4278	3.2142±3.4149
P2D	-0.0529±0.4461	-0.0256±0.3932	-0.0194±0.2275	294.134±131.632

by an ellipse, with the center decided by the mean of the cluster, and the radiuses determined by the eigenvalue of the covariance matrix.

3.1 Euclidean Distance or Mahalanobis Distance

An important issue for the methods that depend on the *k nearest neighbors* is on the searching of k neighbors, which are largely determined by the similarity measure. Traditionally, the Mahalanobis distance is adopted to measure the similarity between two Gaussian distributions. However, it was found in the simulations that the Mahalanobis distance was easily going to magnify the similarity of two Gaussian functions.

An example is shown in Figure 1. It can be seen that $k = 3$ nearest neighbors in the *reference* scan (marked in green five-starts) of a Gaussian component in the *floating* scan (marked in black ellipse) found by Mahalanobis distance are far from the ground truth. However, such a dilemma could be alleviated by the Euclidean distance (see the Gaussian components marked in red diamond in Figure 1). The underlying reason may be that Mahalanobis distance is infeasible for two Gaussian distributions that differ much in the covariance matrix. Note that "FSD" and "SSD" mean the Gaussian distributions of the *floating* and *reference* scan respectively. "ED", "MD" and "MFSD" mark the center of the corresponding Gaussian functions.

3.2 Estimation Precision

The second experiment was used to test the feasibility of the proposed algorithm. Now that ground truth transformation parameters are unavailable between two overlapping sonar scans, we randomly chosen several sonar scans as the *floating* scan, and transform each scan to be the *reference* scan with a random parameter set. Therefore, the precision of the proposed method could be measured by the error between the estimated result and the predefined values. Offsets along x and y axes were randomly distributed in interval $[-4, 4]$ meters, while the rotation ranged in $[-10°,10°]$. A total of 150 tests were generated . The cluster number for the kD2D-NDT method was empirically set to be the point number of a scan divided by 120.

For comparison, the ICP, P2D-NDT and D2D-NDT methods were used to test the efficiency of the proposed kD2D-NDT method. The D2D-NDT and P2D-NDT were performed with iterative optimization at grid sizes of [10;5;2;1] meters and [10;7] meters, respectively. An example for motion parameters estimation is presented in Table 1. It can be seen that the proposed kD2D-NDT method is more accurate than other methods in some cases. The average estimation precision for each method is displayed in Table 2. The results of 20 out of 150 tests where the D2D-NDT diverges are not included in the average estimation precision calculation in Table 2. Though there are 8 out of 150 tests, where the kD2D-NDT outputs [0,0,0] or an obviously wrong result, it can be helped by just restarting the kD2D-NDT algorithm.

From Table 2, it can be seen that the proposed kD2D-NDT method has a comparable performance with other methods. However, the kD2D-NDT method runs faster than the rest of algorithms. P2D-NDT gets the best performance at the cost of runtime much longer than others, because a normal distribution distance has to be calculated for each point in each iteration. All algorithms are implemented in MATLAB 2014a on a 3.2GHz Intel Core i5 processor with 4GB of RAM.

3.3 Scan Mosaicking

The difference between registration results produced by different algorithms is often small. Local registration errors will be accumulated rapidly if consecutive frames are registered to form a panoramic view. The details in the panoramic image will become blurred if the global error is large. In this experiment, we tried to register five consecutive sonar scans. The panoramic images stitched with different algorithms are shown in Figure 2. Observing Figure 2(a) to (c) carefully, one can see that the kD2D-NDT map is sharper than the D2D-NDT map and ICP map in details. When registering the 77th sonar scan to 76th sonar scan, the P2D-NDT converged to a local minimum. The reason behind this phenomenon may be that there is a big gap in 76th sonar scan after distortion correction. However, kD2D-NDT algorithm is feasible for the situation (see Figure 2(a)). It demonstrates that, again, the proposed kD2D-NDT method is validate for the underwater forward-looking sonar image registration.

4 Conclusion And Discussion

In this paper, we tried to register the underwater sonar scans that were taken by the Mechanical Scanning Imaging Sonar with a distribution-to-distribution method, named kD2D-

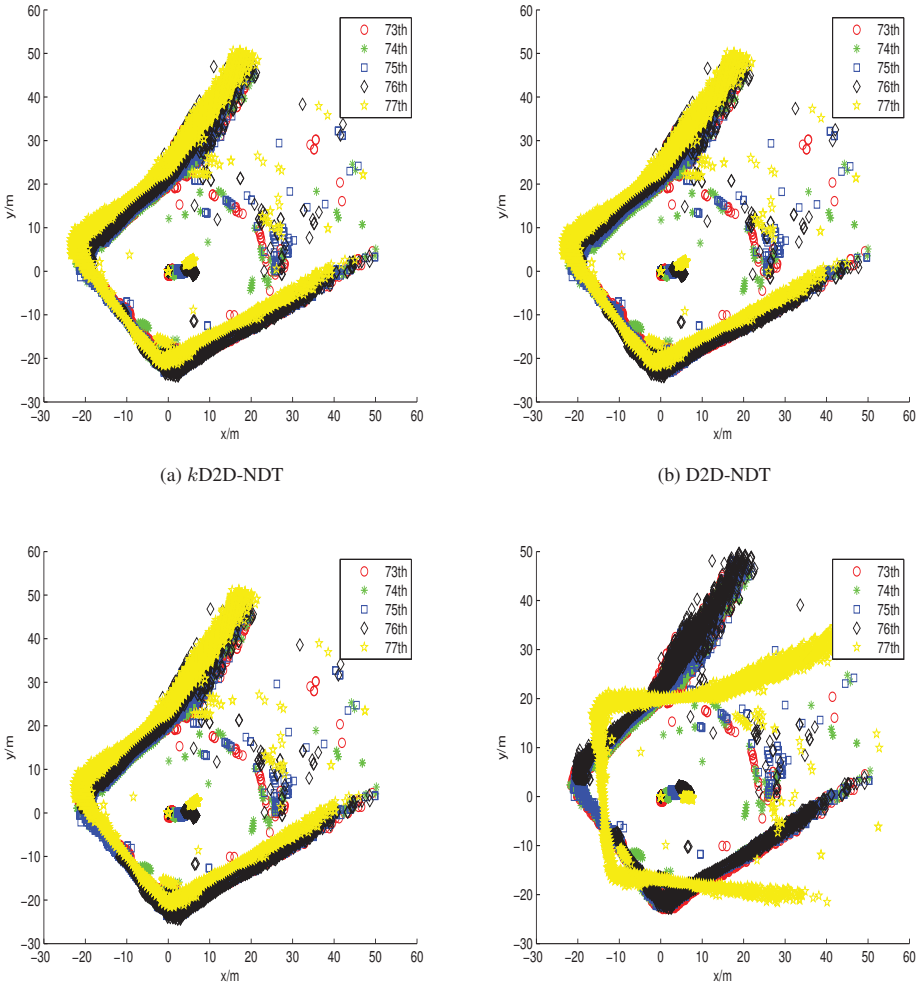

(a) kD2D-NDT (b) D2D-NDT

(c) ICP (d) P2D-NDT

Figure 2: Register five consecutive scans to form a panoramic view with different methods.

NDT algorithm. To better accommodate the Gaussian assumption, we grouped the point clouds in each scan with the *K-means* clustering algorithm. For each Gaussian component in the *floating* scan, only k nearest Gaussian components in the *reference* scan were chosen to measure the similarity. The number of Gaussian components was experimentally set to be 3. The Euclidean distance was adopted to search for the Gaussian component pairs between the *floating* scan and the *reference* scan. Analytic expressions for the gradient and Hessian matrix of the objective function were presented and the Newtonian descending method was adopted to find the local minimum.

A few issues still remain open. Firstly, *K-means* clustering algorithm randomly selects the clustering center. Although the input point set is same, the clustering results are different every time. This factor plays an important impact on the kD2D-NDT registration algorithm. Sometimes, the registration algorithm diverges or it takes long time to converge to the minimum. Secondly, the initial guess is very important to make the registration algorithm converge to the global minimum. Thirdly, the scattering points sensibly affect the distribution of the clustering result, making the covariance of the clustering results be world apart, although the input point set is same. This enormous difference will weaken other distributions power in the registration process, sometimes causing divergence.

It should be noted that no feature extraction step appears in the current registration framework, though the dataset was collected from a structured environment. Compared to P2D-NDT and D2D-NDT, no iterative optimization at different grid size is needed, further accelerating speed. In the future, we will test the algorithm with the dataset collected from fully unstructured environment. Furthermore, we will improve the accuracy, speed and robustness of the proposed algorithm. For example, strategies will be designed to remove the scattering points. On another hand, a better clustering or division method will be proposed to better satisfy the Gaussian assumption.

REFERENCES

[1] S.B. Williams, O. Pizarro, J. Webster, R. Beaman, M. Johnson-Roberson, et al., AUV-assisted Surveying of Relic Reef Sites. Oceans 2008, 1-7, 2008.

[2] I. Mahon, O. Pizarro, M. Johnson-Roberson, A. Friedman, S.B. Williams, et al., Reconstructing Pavlopetri: Mapping the World's Oldest Submerged Town using Stereo-vision. 2011 Ieee International Conference on Robotics and Automation (Icra), 2315-2321, 2011.

[3] S. F. J., R. A. F., V. A. Sebastin and A. G. G., Artificial Potential Fields for the obstacles avoidance system of an AUV using a Mechanical Scanning Sonar. 2016 3rd Ieee/Oes South American International Symposium on Oceanic Engineering (Saisoe), 1-6, 2016.

[4] M. Zhou, R. Bachmayer and B. deYoung, Towards Autonomous Underwater Iceberg Profiling using a Mechanical Scanning Sonar on a Underwater Slocum Glider. 2016 Ieee/Oes Autonomous Underwater Vehicles (Auv), 101-107,2016.

[5] A. Mallios, P. Ridao, D. Ribas, M. Carreras and R. Camilli, Toward Autonomous Exploration in Confined Underwater Environments. Journal of Field Robotics, Vol.33, No.7, 994-1012, 2016.

[6] Hurtos, N., X. Cuf', Y. Petillot and J. Salvi. Fourier-based registrations for two-dimensional forward-looking sonar image mosaicing. in Ieee/rsj International Conference on Intelligent Robots and Systems. 2012.

[7] Hurtos, N., D. Ribas, X. Cufi, Y. Petillot and J. Salvi, Fourier-based Registration for Robust Forward-looking Sonar Mosaicing in Low-visibility Underwater Environments. Journal of Field Robotics, Vol.32, No.1, 123-151, 2015.

[8] Song, S., J.M. Herrmann, K. Liu, S. Li and X. Feng. Forward-looking sonar image mosaicking by feature tracking. in IEEE International Conference on Robotics and Biomimetics, 1613-1618, 2017.

[9] Song, S.M., J.M. Herrmann, B.L. Si, K.Z. Liu and X.S. Feng, Two-dimensional forward-looking sonar image registration by maximization of peripheral mutual information. International Journal of Advanced Robotic Systems, Vol.14, No.6, 1-17, 2017.

[10] B. He, H.J. Zhang, C. Li, S.J. Zhang, Y. Liang, et al., Autonomous Navigation for Autonomous Underwater Vehicles Based on Information Filters and Active Sensing. Sensors, Vol.11, No.11, 10958-10980, 2011.

[11] D. Ribas, P. Ridao, J.D. Tardos and J. Neira, Underwater SLAM in Man-Made Structured Environments. Journal of Field Robotics, Vol.25, No.11-12, 898-921, 2008.

[12] U. Castellani, A. Fusiello, V. Murino and L. Papaleo. Efficient on-line mosaicing from 3D acoustical images. in Oceans '04. Mtts/ieee Techno-Ocean. Vol.2, 670-677, 2004.

[13] E. Hernndez, P. Ridao, D. Ribas and A. Mallios, Probabilistic Sonar Scan Matching for an AUV. 2009 Ieee-Rsj International Conference on Intelligent Robots and Systems, 255-260, 2009.

[14] H. Buelow, Using Robust Spectral Registration for Scan Matching of Sonar Range Data. IFAC Proceedings Volumes, Vol.43, No.16, 611-616, 2010.

[15] H. Bulow, A. Birk, Spectral registration of noisy sonar data for underwater 3D mapping. Autonomous Robots, Vol.30, No.3, 307-331, 2011.

[16] L. Chen, S. Wang, H.S. Hu, D.B. Gu, L.Q. Liao, Improving Localization Accuracy for an Underwater Robot With a Slow-Sampling Sonar Through Graph Optimization. Ieee Sensors Journal, Vol.15, No.9, 5024-5035, 2015.

[17] P. Biber, The normal distributions transform: A new approach to laser scan matching. Iros 2003: Proceedings of the 2003 Ieee/Rsj International Conference on Intelligent Robots and Systems, Vols.1-4, 2743-2748, 2003.

[18] T.D. Stoyanov, M. Magnusson, H. Andreasson, A.J. Lilienthal, Fast and Accurate Scan Registration through Minimization of the Distance between Compact 3D NDT Representations. International Journal of Robotics Research, Vol.31, No.12, 1377-1393, 2012.

[19] D. Ribas, Dataset obtained in an abandoned marina.[Online]. Available:http://cres.usc.edu/radishrepository/view-one.php?name=abandoned_marina.

[20] A. Mallios, P. Ridao, D. Ribas, E. Hernndez, Scan matching SLAM in underwater environments. Autonomous Robots, Vol.36, No.3, 181-198, 2014.